

A POSTERIORI VIRTUAL ELEMENT METHOD FOR THE ACOUSTIC VIBRATION PROBLEM

F. LEPE, D. MORA, G. RIVERA, AND I. VELÁSQUEZ

ABSTRACT. In two dimensions, we propose and analyze an a posteriori error estimator for the acoustic spectral problem based on the virtual element method in $H(\operatorname{div}; \Omega)$. Introducing an auxiliary unknown, we use the fact that the primal formulation of the acoustic problem is equivalent to a mixed formulation, in order to prove a superconvergence result, necessary to dispense high order terms. Under the virtual element approach, we prove that our local indicator is reliable and globally efficient in the L^2 -norm. We provide numerical results to assess the performance of the proposed error estimator.

1. INTRODUCTION

One of the most important subjects in the development of numerical methods for partial differential equations is the a posteriori error analysis, since it allows dealing with singular solutions that arise due, for instance, geometrical features of the domain or some particular boundary conditions, among others. In this sense, and in particular for eigenvalue problems arising from problems related to solid and fluid mechanics and electromagnetism, just to mention some possible applications, the a posteriori analysis has taken relevance in recent years. (see [2, 12, 14, 11, 21, 22, 33, 35, 38, 39] and the references therein).

The virtual element method (VEM), introduced in [4], has shown remarkable results in different problems, and particularly for solving eigenproblems, showing great accuracy and flexibility in the approximation of eigenvalues and eigenfunctions. We mention [18, 19, 24, 25, 26, 27, 28, 31, 30, 32, 33, 34, 36] as recent works on this topic.

The acoustic vibration problem appears in important applications in engineering. In fact, it can be used to design of structures and devices for noise reduction in aircraft or cars mainly related with solid-structure interaction problems, among others important applications. In the last years, several numerical methods have been developed in order to approximate the eigenpairs of the associated spectral problem. In particular, a virtual element discretization has been proposed in [9]. It is well known that one of the most important features of the virtual element method is the efficient computational implementation and the flexibility on the geometries for meshes, where precisely adaptivity strategies can be implemented in an easy way. In fact, the hanging nodes that appear in the refinement of some element of the mesh, can be treated as new nodes since adjacent non matching element interfaces are acceptable in the VEM. Recent research papers report interesting advantages of the VEM in the a posteriori error analysis and adaptivity for source problems. We refer to [7, 16, 17, 37] and the references therein, for instance, for a further discussion. On the other hand, a posteriori error analysis

2000 *Mathematics Subject Classification.* 65N30, 65N25, 70J30, 76M25.

Key words and phrases. virtual element method, acoustic vibration problem, polygonal meshes, a posteriori error estimates, superconvergence.

The first author has been partially supported by DICREA through project 2120173 GI/C Universidad del Bío-Bío and ANID-Chile through FONDECYT project 11200529, Chile.

The second author was partially supported by DICREA through project 2120173 GI/C Universidad del Bío-Bío, by the National Agency for Research and Development, ANID-Chile through FONDECYT project 1220881, by project ANILLO OF COMPUTATIONAL MATHEMATICS FOR DESALINATION PROCESSES ACT210087, and by project project Centro de Modelamiento Matemático (CMM), ACE210010 and FB210005, BASAL funds for centers of excellence.

The third author was supported by through project R02/21 Universidad de Los Lagos.

for eigenproblems by VEM have been recently introduced in [40, 33, 35], where primal formulations in H^1 have been considered.

The contribution of our work is the design and analysis of an a posteriori error estimator for the acoustic spectral problem, by means of a VEM method. The VEM that we consider in our analysis is the one introduced in [9] for the a priori error analysis of the acoustic eigenproblem. We stress that the VEM method presented in [9] may be preferable to more standard finite elements even in the case of triangular meshes in terms of dofs (cf. [9, Remark 3]). The formulation for the acoustic problem is written only in terms of the displacement of the fluid, which leads to a bilinear form with divergence terms, implying that the analysis for the a posteriori error indicator is not straightforward. This difficulty produced by the $H(\text{div})$ formulations leads to analyze, in first place, an equivalent mixed formulation which provides suitable results in order to control the so-called high order terms that naturally appear. This analysis depending on an equivalent mixed formulation has been previously considered in [13, 14] for the a posteriori analysis for the Maxwell's eigenvalue problem, inspired by the superconvergence results of [29] for mixed spectral formulations. We will follow the same techniques for the present $H(\text{div})$ framework. However, due to the nature of the VEM, the local indicator that we present contains an extra term depending on the virtual projector which needs to be analyzed carefully.

The organization of our paper is the following: in section 2 we present the acoustic problem and the mixed equivalent formulation for it. We recall some properties of the spectrum of the spectral problem and regularity results. In section 3 we found the core of the analysis of our paper, where we introduce the virtual element method for our spectral problem and technical results that will be needed to establish a superconvergence result, with the aid of mixed formulations. Section 4 is dedicated to the a posteriori error analysis, where we introduce our local and global indicators which, as is customary in the posteriori error analysis, will be reliable and efficient. In section 5, we report numerical tests where we assess the performance of our estimator. We end the article with some concluding remarks.

Throughout this work, Ω is a generic Lipschitz bounded domain of \mathbb{R}^2 . For $s \geq 0$, $\|\cdot\|_{s,\Omega}$ stands indistinctly for the norm of the Hilbertian Sobolev spaces $H^s(\Omega)$ or $[H^s(\Omega)]^2$ with the convention $H^0(\Omega) := L^2(\Omega)$. We also define the Hilbert space $H(\text{div}; \Omega) := \{\boldsymbol{\tau} \in [L^2(\Omega)]^2 : \text{div } \boldsymbol{\tau} \in L^2(\Omega)\}$, whose norm is given by $\|\boldsymbol{\tau}\|_{\text{div},\Omega}^2 := \|\boldsymbol{\tau}\|_{0,\Omega}^2 + \|\text{div } \boldsymbol{\tau}\|_{0,\Omega}^2$. For $s \geq 0$, we define the Hilbert space $H^s(\text{div}; \Omega) := \{\boldsymbol{\tau} \in [H^s(\Omega)]^2 : \text{div } \boldsymbol{\tau} \in H^s(\Omega)\}$, whose norm is given by $\|\boldsymbol{\tau}\|_{H^s(\text{div};\Omega)}^2 := \|\boldsymbol{\tau}\|_{s,\Omega}^2 + \|\text{div } \boldsymbol{\tau}\|_{s,\Omega}^2$. Finally, we employ $\mathbf{0}$ to denote a generic null vector and the relation $\mathbf{a} \lesssim \mathbf{b}$ indicates that $\mathbf{a} \leq C\mathbf{b}$, with a positive constant C which is independent of \mathbf{a} , \mathbf{b} , and the size of the elements in the mesh. The value of C might change at each occurrence. We remark that we will write the constant C only when is needed.

2. THE SPECTRAL PROBLEM

We consider the free vibration problem for an acoustic fluid within a bounded rigid cavity $\Omega \subset \mathbb{R}^2$ with polygonal boundary Γ and outward unit normal vector \mathbf{n} :

$$(1) \quad \begin{cases} -\omega^2 \varrho \mathbf{w} = -\nabla p & \text{in } \Omega, \\ p = -\varrho c^2 \text{div } \mathbf{w} & \text{in } \Omega, \\ \mathbf{w} \cdot \mathbf{n} = 0 & \text{on } \Gamma, \end{cases}$$

where \mathbf{w} is the fluid displacement, p is the pressure fluctuation, ϱ the density, c the acoustic speed and ω the vibration frequency. For simplicity on the forthcoming analysis, we consider ϱ and c equal to one.

Multiplying the first equation in (1) by a test function $\boldsymbol{\tau} \in H_0(\text{div}; \Omega)$, where

$$H_0(\text{div}; \Omega) := \{\boldsymbol{\tau} \in H(\text{div}; \Omega) : \boldsymbol{\tau} \cdot \mathbf{n} = 0 \text{ on } \Gamma\},$$

integrating by parts, using the boundary condition and eliminating the pressure p , we arrive at the following weak formulation

Problem 2.1. Find $(\lambda, \mathbf{w}) \in \mathbb{R} \times H_0(\text{div}; \Omega)$, $\mathbf{w} \neq 0$, such that

$$\int_{\Omega} \text{div } \mathbf{w} \text{ div } \boldsymbol{\tau} = \lambda \int_{\Omega} \mathbf{w} \cdot \boldsymbol{\tau} \quad \forall \boldsymbol{\tau} \in H_0(\text{div}; \Omega),$$

where $\lambda := \omega^2$. It is well known that the spectrum of Problem 2.1 consists in a sequence of eigenvalues $\{0\} \cup \{\lambda_k\}_{k \in \mathbb{N}}$, such that

- i) $\lambda = 0$ is an infinite-multiplicity eigenvalue and its associated eigenspace is $H_0(\text{div}^0; \Omega) := \{\boldsymbol{\tau} \in H_0(\text{div}; \Omega) : \text{div } \boldsymbol{\tau} = 0 \text{ in } \Omega\}$;
- ii) $\{\lambda_k\}_{k \in \mathbb{N}}$ is a sequence of finite-multiplicity eigenvalues which satisfy $\lambda_k \rightarrow \infty$.

To perform an a posteriori error analysis for spectral problems, we need the so called *superconvergence result*, in order to neglect high order terms as has been proved in [29] and already applied in, for instance, the Maxwell's eigenvalue problem [13, 14]. In order to obtain this superconvergence result, we begin by introducing an equivalent mixed formulation for Problem 2.1. For $\lambda \neq 0$ let us introduce the unknown

$$(2) \quad u := -\frac{\text{div } \mathbf{w}}{\lambda} \in L^2(\Omega).$$

To remain consistent with the notations, we will denote by $(\cdot, \cdot)_{0, \Omega}$ the $L^2(\Omega)$ inner-product.

With the aid of (2) we write the following mixed eigenproblem:

Problem 2.2. Find $(\lambda, \mathbf{w}, u) \in \mathbb{R} \times H_0(\text{div}; \Omega) \times L^2(\Omega)$, with $(\mathbf{w}, u) \neq \mathbf{0}$, such that

$$\begin{cases} \int_{\Omega} \mathbf{w} \cdot \boldsymbol{\tau} + \int_{\Omega} u \text{ div } \boldsymbol{\tau} = 0 & \forall \boldsymbol{\tau} \in H_0(\text{div}; \Omega), \\ \int_{\Omega} v \text{ div } \mathbf{w} = -\lambda \int_{\Omega} uv & \forall v \in L^2(\Omega). \end{cases}$$

It is easy to check that the spectral Problem 2.1 and 2.2 are equivalent, except for $\lambda = 0$ on the following sense:

- If (λ, \mathbf{w}) is a solution of Problem 2.1, with $\lambda \neq 0$, then $(\lambda, \mathbf{w}, -\text{div } \mathbf{w}/\lambda)$ is solution of Problem 2.2.
- If (λ, \mathbf{w}, u) is a solution of Problem 2.2, then (λ, \mathbf{w}) is solution of Problem 2.1 and u is defined as in (2).

We introduce the bounded and symmetric bilinear forms $a : H_0(\text{div}; \Omega) \times H_0(\text{div}; \Omega) \rightarrow \mathbb{R}$ and $b : H_0(\text{div}; \Omega) \times L^2(\Omega) \rightarrow \mathbb{R}$, defined by

$$a(\mathbf{w}, \boldsymbol{\tau}) := \int_{\Omega} \mathbf{w} \cdot \boldsymbol{\tau}, \quad \mathbf{w}, \boldsymbol{\tau} \in H_0(\text{div}; \Omega), \quad b(\boldsymbol{\tau}, v) := \int_{\Omega} v \text{ div } \boldsymbol{\tau}, \quad \boldsymbol{\tau} \in H_0(\text{div}; \Omega), v \in L^2(\Omega),$$

which allows us to we rewrite Problem 2.2 as follows:

Problem 2.3. Find $(\lambda, \mathbf{w}, u) \in \mathbb{R} \times H_0(\text{div}; \Omega) \times L^2(\Omega)$, $(\mathbf{w}, u) \neq (\mathbf{0}, 0)$, such that

$$\begin{cases} a(\mathbf{w}, \boldsymbol{\tau}) + b(\boldsymbol{\tau}, u) = 0 & \forall \boldsymbol{\tau} \in H_0(\text{div}; \Omega), \\ b(\mathbf{w}, v) = -\lambda(u, v)_{0, \Omega} & \forall v \in L^2(\Omega). \end{cases}$$

Remark 2.1. It is easy to check that if $(\lambda, \mathbf{w}, \mathbf{u})$ is a solution of Problem 2.3, then

$$\mathbf{w} = \nabla u \quad \text{and} \quad \text{div } \mathbf{w} = -\lambda u.$$

Let \mathcal{K} be the kernel of bilinear form $b(\cdot, \cdot)$ defined by:

$$\mathcal{K} := \{\boldsymbol{\tau} \in H_0(\text{div}; \Omega) : \text{div } \boldsymbol{\tau} = 0 \text{ in } \Omega\}.$$

It is well-known that bilinear form $a(\cdot, \cdot)$ is elliptic in \mathcal{K} and that $b(\cdot, \cdot)$ satisfies the following inf-sup condition (see [10])

$$(3) \quad \sup_{\mathbf{0} \neq \boldsymbol{\tau} \in H_0(\text{div}; \Omega)} \frac{b(\boldsymbol{\tau}, v)}{\|\boldsymbol{\tau}\|_{\text{div}, \Omega}} \geq \beta \|v\|_{0, \Omega} \quad \forall v \in L^2(\Omega),$$

where β is a positive constant.

Remark 2.2. *The eigenvalues of Problem 2.3 are positive. Indeed, taking $\boldsymbol{\tau} = \mathbf{w}$ and $v = u$ in Problem 2.3 and subtracting the resulting forms, we obtain*

$$\lambda = \frac{a(\mathbf{w}, \mathbf{w})}{\|u\|_{0,\Omega}^2} \geq 0.$$

In addition, $\lambda = 0$ implies $(\mathbf{w}, u) = (\mathbf{0}, 0)$.

Let us introduce the following source problem: For a given $g \in L^2(\Omega)$, the pair $(\tilde{\mathbf{w}}, \tilde{u}) \in H_0(\text{div}; \Omega) \times L^2(\Omega)$ is the solution of the following well posed problem

$$\begin{aligned} (4) \quad & a(\tilde{\mathbf{w}}, \boldsymbol{\tau}) + b(\boldsymbol{\tau}, \tilde{u}) = 0 \quad \forall \boldsymbol{\tau} \in H_0(\text{div}; \Omega), \\ (5) \quad & b(\tilde{\mathbf{w}}, v) = -(g, v)_{0,\Omega} \quad \forall v \in L^2(\Omega). \end{aligned}$$

According to [1], the regularity for the solution of system (4)–(5), (the associated source problem to Problem 2.3) is the following: there exists a constant $\tilde{r} > 1/2$ depending on Ω such that the solution $\tilde{u} \in H^{1+\tilde{r}}(\Omega)$, where \tilde{r} is at least 1 if Ω is convex and \tilde{r} is at least $\pi/\omega - \varepsilon$, for any $\varepsilon > 0$ for a non-convex domain, with $\omega < 2\pi$ being the largest reentrant angle of Ω . Hence we have the following well known additional regularity result for the source problem (4)–(5).

$$(6) \quad \|\tilde{\mathbf{w}}\|_{\tilde{r},\Omega} + \|\tilde{u}\|_{1+\tilde{r},\Omega} \lesssim \|g\|_{0,\Omega}.$$

Also, the eigenvalues are well characterized for this problem as is stated in the following result (see [3] for instance).

Lemma 2.1. *The eigenvalues of Problem 2.2 consist in a sequence of positive eigenvalues $\{\lambda_n : n \in \mathbb{N}\}$, such that $\lambda_n \rightarrow \infty$ as $n \rightarrow \infty$. In addition, the following additional regularity result holds true for eigenfunctions*

$$\|\mathbf{w}\|_{r,\Omega} + \|\text{div } \mathbf{w}\|_{1+r,\Omega} + \|u\|_{1+r,\Omega} \lesssim \|u\|_{0,\Omega},$$

with $r > 1/2$ and the hidden constant depending on the eigenvalue.

3. THE VIRTUAL ELEMENT DISCRETIZATION

We begin this section recalling the mesh construction and the assumptions considered to introduce the discrete virtual element space. Then, we will introduce a virtual element discretization of Problem 2.1 and provide a spectral characterization of the resulting discrete eigenvalue problem.

Let $\{\mathcal{T}_h\}_h$ be a sequence of decompositions of Ω into polygons K . Let h_K denote the diameter of the element K and $h := \max_{K \in \Omega} h_K$. For the analysis, the following standard assumptions on the meshes are considered (see [5, 15]): there exists a positive real number $C_{\mathcal{T}}$ such that, for every $K \in \mathcal{T}_h$ and for every h .

A₁: the ratio between the shortest edge and the diameter h_K of K is larger than $C_{\mathcal{T}}$,

A₂: $K \in \mathcal{T}_h$ is star-shaped with respect to every point of a ball of radius $C_{\mathcal{T}}h_K$.

For any subset $S \subseteq \mathbb{R}^2$ and nonnegative integer k , we indicate by $\mathbb{P}_k(S)$ the space of polynomials of degree up to k defined on S . To keep the notation simpler, we denote by \mathbf{n} a general normal unit vector, its precise definition will be clear from the context. We consider now a polygon K and define the following local finite dimensional space for $k \geq 0$ (see [15, 5]):

$$\mathbf{H}_h^K := \{\boldsymbol{\tau}_h \in H(\text{div}; K) \cap H(\text{rot}; K) : (\boldsymbol{\tau}_h \cdot \mathbf{n}) \in \mathbb{P}_k(\ell) \forall \ell \in \partial K, \text{div } \boldsymbol{\tau}_h \in \mathbb{P}_k(K), \text{rot } \boldsymbol{\tau}_h = 0 \text{ on } K\},$$

We define the following degrees of freedom for functions $\boldsymbol{\tau}_h$ in \mathbf{H}_h^K :

$$(7) \quad \int_{\ell} (\boldsymbol{\tau}_h \cdot \mathbf{n}) q \, ds \quad \forall q \in \mathbb{P}_k(\ell) \quad \forall \text{edge } \ell \in \partial K,$$

$$(8) \quad \int_K \boldsymbol{\tau}_h \cdot \nabla q \quad \forall q \in \mathbb{P}_k(K)/\mathbb{P}_0(K),$$

which are unisolvent (see [9, Proposition 1]).

For every decomposition \mathcal{T}_h of Ω into polygons K , we define

$$\mathbf{H}_h := \left\{ \boldsymbol{\tau}_h \in \mathbf{H}_0(\operatorname{div}; \Omega) : \boldsymbol{\tau}_h|_K \in \mathbf{H}_h^K \right\}.$$

In agreement with the local choice we choose the following degrees of freedom:

$$\begin{aligned} \int_{\ell} (\boldsymbol{\tau}_h \cdot \mathbf{n}) q \, ds & \quad \forall q \in \mathbb{P}_k(\ell) \quad \text{for all internal edges } \ell \in \mathcal{T}_h, \\ \int_K \boldsymbol{\tau}_h \cdot \nabla q & \quad \forall q \in \mathbb{P}_k(K)/\mathbb{P}_0(K) \quad \text{in each element } K \in \mathcal{T}_h. \end{aligned}$$

In order to construct the discrete scheme, we need some preliminary definitions. For each element $K \in \mathcal{T}_h$, we define the space

$$\widehat{\mathbf{H}}_h^K := \nabla(\mathbb{P}_{k+1}(K)) \subset \mathbf{H}_h^K.$$

Next, we define the orthogonal projector $\boldsymbol{\Pi}_h^K : [L^2(K)]^2 \rightarrow \widehat{\mathbf{H}}_h^K$ by

$$(9) \quad \int_K \boldsymbol{\Pi}_h^K \boldsymbol{\tau} \cdot \widehat{\mathbf{u}}_h = \int_K \boldsymbol{\tau} \cdot \widehat{\mathbf{u}}_h \quad \forall \widehat{\mathbf{u}}_h \in \widehat{\mathbf{H}}_h^K,$$

and we point out that $\boldsymbol{\Pi}_h^K \boldsymbol{\tau}_h$ is explicitly computable for every $\boldsymbol{\tau}_h \in \mathbf{H}_h^K$ using only its degrees of freedom (7)–(8). In fact, it is easy to check that, for all $\boldsymbol{\tau}_h \in \mathbf{H}_h^K$ and for all $q \in \mathbb{P}_{k+1}(K)$,

$$\int_K \boldsymbol{\Pi}_h^K \boldsymbol{\tau}_h \cdot \nabla q = \int_K \boldsymbol{\tau}_h \cdot \nabla q = - \int_K q \operatorname{div} \boldsymbol{\tau}_h + \int_{\partial K} (\boldsymbol{\tau}_h \cdot \mathbf{n}) q \, ds.$$

On the other hand, let $S^K(\cdot, \cdot)$ be any symmetric positive definite (and computable) bilinear form that satisfies

$$(10) \quad c_0 \int_K \boldsymbol{\tau}_h \cdot \boldsymbol{\tau}_h \leq S^K(\boldsymbol{\tau}_h, \boldsymbol{\tau}_h) \leq c_1 \int_K \boldsymbol{\tau}_h \cdot \boldsymbol{\tau}_h \quad \forall \boldsymbol{\tau}_h \in \mathbf{H}_h^K,$$

for some positive constants c_0 and c_1 depending only on the shape regularity constant $C_{\mathcal{T}}$ from mesh assumptions \mathbf{A}_1 and \mathbf{A}_2 . Then, we define on each K the following bilinear form:

$$a_h^K(\mathbf{u}_h, \boldsymbol{\tau}_h) := \int_K \boldsymbol{\Pi}_h^K \mathbf{u}_h \cdot \boldsymbol{\Pi}_h^K \boldsymbol{\tau}_h + S^K(\mathbf{u}_h - \boldsymbol{\Pi}_h^K \mathbf{u}_h, \boldsymbol{\tau}_h - \boldsymbol{\Pi}_h^K \boldsymbol{\tau}_h) \quad \mathbf{u}_h, \boldsymbol{\tau}_h \in \mathbf{H}_h^K,$$

and, in a natural way,

$$a_h(\mathbf{u}_h, \boldsymbol{\tau}_h) := \sum_{K \in \mathcal{T}_h} a_h^K(\mathbf{u}_h, \boldsymbol{\tau}_h), \quad \mathbf{u}_h, \boldsymbol{\tau}_h \in \mathbf{H}_h.$$

The following properties of the bilinear form $a_h^K(\cdot, \cdot)$ are easily derived (by repeating, in our case, the arguments from [15, Proposition 4.1]).

- *Consistency:*

$$a_h^K(\widehat{\mathbf{u}}_h, \boldsymbol{\tau}_h) = \int_K \widehat{\mathbf{u}}_h \cdot \boldsymbol{\tau}_h \quad \forall \widehat{\mathbf{u}}_h \in \widehat{\mathbf{H}}_h^K \quad \forall \boldsymbol{\tau}_h \in \mathbf{H}_h^K, \quad \forall K \in \mathcal{T}_h.$$

- *Stability:* There exist two positive constants α_* and α^* , independent of K , such that:

$$\alpha_* \int_K \boldsymbol{\tau}_h \cdot \boldsymbol{\tau}_h \leq a_h^K(\boldsymbol{\tau}_h, \boldsymbol{\tau}_h) \leq \alpha^* \int_K \boldsymbol{\tau}_h \cdot \boldsymbol{\tau}_h \quad \forall \boldsymbol{\tau}_h \in \mathbf{H}_h^K, \quad \forall K \in \mathcal{T}_h.$$

Now, we are in position to write the virtual element discretization of Problem 2.1.

Problem 3.1. Find $(\lambda_h, \mathbf{w}_h) \in \mathbb{R} \times \mathbf{H}_h$, $\mathbf{w}_h \neq 0$ such that

$$(\operatorname{div} \mathbf{w}_h, \operatorname{div} \boldsymbol{\tau}_h)_{0,\Omega} = \lambda_h a_h(\mathbf{w}_h, \boldsymbol{\tau}_h) \quad \forall \boldsymbol{\tau}_h \in \mathbf{H}_h.$$

We have the following spectral characterization of the discrete eigenvalue Problem 3.1 (see [9]).

Remark 3.1. *There exist $M_h := \dim(\mathbf{H}_h)$ eigenvalues of Problem 3.1 repeated according to their respective multiplicities, which are $\{0\} \cup \{\lambda_{hk}\}_{k=1}^{N_h}$, where:*

- i) the eigenspace associated with $\lambda_h = 0$ is $\mathcal{K}_h := \{\mathbf{v}_h \in \mathbf{H}_h : \operatorname{div} \mathbf{v}_h = 0\}$;*
- ii) $\lambda_{hk} > 0$, $k = 1, \dots, N_h := M_h - \dim(\mathcal{K}_h)$, are non-defective eigenvalues repeated according to their respective multiplicities.*

Now, we introduce the virtual element discretization of Problem 2.3.

Problem 3.2. *Find $(\lambda_h, \mathbf{w}_h, u_h) \in \mathbb{R} \times \mathbf{H}_h \times \mathbf{Q}_h$, $(\mathbf{w}_h, u_h) \neq (\mathbf{0}, 0)$, such that*

$$\begin{cases} a_h(\mathbf{w}_h, \boldsymbol{\tau}_h) + b(\boldsymbol{\tau}_h, u_h) &= 0 & \forall \boldsymbol{\tau}_h \in \mathbf{H}_h, \\ b(\mathbf{w}_h, v_h) &= -\lambda_h(u_h, v_h)_{0,\Omega} & \forall v_h \in \mathbf{Q}_h, \end{cases}$$

where $\mathbf{Q}_h := \{q \in L^2(\Omega) : q|_K \in \mathbb{P}_k(K) \quad \forall K \in \mathcal{T}_h\}$, $k \geq 0$.

We also introduce the $L^2(\Omega)$ -orthogonal projection

$$P_k : L^2(\Omega) \rightarrow \mathbf{Q}_h,$$

and the following approximation result (see [5]): if $0 \leq s \leq k+1$, it holds

$$(11) \quad \|v - P_k v\|_{0,\Omega} \lesssim h^s \|v\|_{s,\Omega} \quad \forall v \in H^s(\Omega).$$

The next two technical results establish the approximation properties for $\boldsymbol{\tau}_I$ and their proofs can be found in [9, Appendix].

Lemma 3.1. *Let $\boldsymbol{\tau} \in H_0(\operatorname{div}; \Omega)$ be such that $\boldsymbol{\tau} \in [H^t(\Omega)]^2$ with $t > 1/2$. There exists $\boldsymbol{\tau}_I \in \mathbf{H}_h$ that satisfies:*

$$\operatorname{div} \boldsymbol{\tau}_I = P_k(\operatorname{div} \boldsymbol{\tau}) \quad \text{in } \Omega.$$

Consequently, for all $K \in \mathcal{T}_h$

$$\|\operatorname{div} \boldsymbol{\tau}_I\|_{0,K} \leq \|\operatorname{div} \boldsymbol{\tau}\|_{0,K},$$

and, if $\operatorname{div} \boldsymbol{\tau}|_K \in H^\delta(K)$ with $\delta \geq 0$, then

$$\|\operatorname{div} \boldsymbol{\tau} - \operatorname{div} \boldsymbol{\tau}_I\|_{0,K} \lesssim h_K^{\min\{\delta, k+1\}} |\operatorname{div} \boldsymbol{\tau}|_{\delta,K}.$$

Lemma 3.2. *Let $\boldsymbol{\tau} \in H_0(\operatorname{div}; \Omega)$ be such that $\boldsymbol{\tau} \in [H^t(\Omega)]^2$ with $t > 1/2$. Then, there exists $\boldsymbol{\tau}_I \in \mathbf{H}_h$ such that, if $1 \leq t \leq k+1$, there holds*

$$\|\boldsymbol{\tau} - \boldsymbol{\tau}_I\|_{0,K} \lesssim h_K^t |\boldsymbol{\tau}|_{t,K},$$

where the hidden constant is independent of h . Moreover, if $1/2 < t \leq 1$, then

$$\|\boldsymbol{\tau} - \boldsymbol{\tau}_I\|_{0,K} \lesssim h_K^t |\boldsymbol{\tau}|_{t,K} + h_K \|\operatorname{div} \boldsymbol{\tau}\|_{0,K}.$$

Let $\boldsymbol{\Pi}_h$ be defined in $[L^2(\Omega)]^2$ by $(\boldsymbol{\Pi}_h \boldsymbol{\tau})|_K := \boldsymbol{\Pi}_h^K \boldsymbol{\tau}$ for all $K \in \mathcal{T}_h$, where $\boldsymbol{\Pi}_h^K$ is the operator defined in (9), and that satisfies the following result proved in [9, Lemma 8].

Lemma 3.3. *For every $q \in H^{1+t}(\Omega)$ with $1/2 < t \leq k+1$, there holds*

$$\|\nabla q - \boldsymbol{\Pi}_h(\nabla q)\|_{0,\Omega} \lesssim h^t \|\nabla q\|_{t,\Omega}.$$

As a consequence of the previous result we have the following estimate.

Lemma 3.4. *For all $r > \frac{1}{2}$ as in Lemma 2.1, the following error estimate holds*

$$\|\mathbf{w} - \boldsymbol{\Pi}_h \mathbf{w}\|_{0,\Omega} \lesssim h^{\min\{r, k+1\}}.$$

Proof. The proof follows directly from Remark 2.1, Lemma 2.1 and Lemma 3.3. □

The following results gives us the error estimates between the eigenfunctions and eigenvalues of Problems 3.2 and 2.3.

Theorem 3.1. *For all $r > \frac{1}{2}$ as in Lemma 2.1, the following error estimates hold*

$$(12) \quad \begin{aligned} \|\mathbf{w} - \mathbf{w}_h\|_{\text{div},\Omega} + \|u - u_h\|_{0,\Omega} &\lesssim h^{\min\{r,k+1\}}, \\ |\lambda - \lambda_h| &\lesssim h^{2\min\{r,k+1\}}, \end{aligned}$$

where the hidden constants are independent of h .

Proof. The proof follows by repeating the arguments in [27, Theorems 4.2, 4.3 and 4.4]. \square

For the a posteriori error analysis that will be developed in Section 4, we will need the following auxiliary results, which have been adapted from [13, 14].

In what follows, let (λ, \mathbf{w}, u) be a solution of Problem 2.3, where we assume that λ is a simple eigenvalue. Let (\mathbf{w}, u) be an associated eigenfunction which we normalize by taking $\|u\|_{0,\Omega} = 1$. Then, for each mesh \mathcal{T}_h , there exists a solution $(\lambda_h, \mathbf{w}_h, u_h)$ of Problem 3.2 such that λ_h converges to λ , as h goes to zero, $\|u_h\|_{0,\Omega} = 1$, and Theorem 3.1 holds true.

Let us introduce the following well posed source problem with data (λ, u) : Find $(\hat{\mathbf{w}}_h, \hat{u}_h) \in \mathbf{H}_h \times \mathbf{Q}_h$, such that

$$(13) \quad \begin{cases} a_h(\hat{\mathbf{w}}_h, \boldsymbol{\tau}_h) + b(\boldsymbol{\tau}_h, \hat{u}_h) &= 0 & \forall \boldsymbol{\tau}_h \in \mathbf{H}_h, \\ b(\hat{\mathbf{w}}_h, v_h) &= -\lambda(u, v_h)_{0,\Omega} & \forall v_h \in \mathbf{Q}_h. \end{cases}$$

With this mixed problem at hand, we will prove the following technical lemmas with the goal of derive a superconvergence result for our VEM. To make matters precise, the forthcoming analysis is inspired by [14], where the authors have generalized the results previously obtained by [10, 20, 23]. We begin proving a higher-order approximation between \hat{u}_h and $P_k u$.

Lemma 3.5. *Let (λ, \mathbf{w}, u) be a solution of Problem 2.3 and $(\hat{\mathbf{w}}_h, \hat{u}_h)$ be a solution of the mixed formulation (13). Then, there holds*

$$\|\hat{u}_h - P_k u\|_{0,\Omega} \lesssim h^{\tilde{r}} (\|\mathbf{w} - \hat{\mathbf{w}}_h\|_{\text{div},\Omega} + \|\mathbf{w} - \mathbf{\Pi}_h \mathbf{w}\|_{0,\Omega}),$$

where $\tilde{r} \in (\frac{1}{2}, 1]$ and the hidden constant is independent of h .

Proof. Let $(\tilde{\mathbf{w}}, \tilde{u}) \in H_0(\text{div}; \Omega) \times L^2(\Omega)$ be the unique solution of the following well posed mixed problem

$$(14) \quad \begin{cases} a(\tilde{\mathbf{w}}, \boldsymbol{\tau}) + b(\boldsymbol{\tau}, \tilde{u}) &= 0 & \forall \boldsymbol{\tau} \in H_0(\text{div}; \Omega), \\ b(\tilde{\mathbf{w}}, v) &= -(\hat{u}_h - P_k u, v)_{0,\Omega} & \forall v \in L^2(\Omega). \end{cases}$$

Notice that (14) is exactly problem (4)–(5) with datum $\hat{u}_h - P_k u$. Hence, since this problem is well posed, we have the following regularity result, consequence of (6)

$$(15) \quad \|\tilde{\mathbf{w}}\|_{\tilde{r},\Omega} + \|\tilde{u}\|_{1+\tilde{r},\Omega} \lesssim \|\hat{u}_h - P_k u\|_{0,\Omega}.$$

Observe that, thanks to the definition of P_k , the first equation of Problem 2.3, and the first equation of (13), we have

$$(16) \quad \begin{aligned} \|\hat{u}_h - P_k u\|_{0,\Omega}^2 &= -b(\tilde{\mathbf{w}}, \hat{u}_h - P_k u) = -b(\tilde{\mathbf{w}}_I, \hat{u}_h - P_k u) = -b(\tilde{\mathbf{w}}_I, \hat{u}_h - u) \\ &= -b(\tilde{\mathbf{w}}_I, \hat{u}_h) + b(\tilde{\mathbf{w}}_I, u) = a_h(\hat{\mathbf{w}}_h, \tilde{\mathbf{w}}_I) - a(\mathbf{w}, \tilde{\mathbf{w}}_I). \end{aligned}$$

In the last two terms of (16), we add and subtract $\mathbf{\Pi}_h \mathbf{w}$ in order to obtain

$$\begin{aligned} a_h(\hat{\mathbf{w}}_h, \tilde{\mathbf{w}}_I) - a(\mathbf{w}, \tilde{\mathbf{w}}_I) &= \underbrace{a_h(\hat{\mathbf{w}}_h - \mathbf{\Pi}_h \mathbf{w}, \tilde{\mathbf{w}}_I) + a(\mathbf{\Pi}_h \mathbf{w} - \hat{\mathbf{w}}_h, \tilde{\mathbf{w}}_I)}_{A_I} + a(\hat{\mathbf{w}}_h - \mathbf{w}, \tilde{\mathbf{w}}_I) \\ &= A_I + \underbrace{a(\hat{\mathbf{w}}_h - \mathbf{w}, \tilde{\mathbf{w}}_I - \tilde{\mathbf{w}})}_{A_{II}} + a(\hat{\mathbf{w}}_h - \mathbf{w}, \tilde{\mathbf{w}}) \\ &= A_I + A_{II} - b(\hat{\mathbf{w}}_h - \mathbf{w}, \tilde{u}) \\ &= A_I + A_{II} - b(\hat{\mathbf{w}}_h - \mathbf{w}, \tilde{u} - P_k \tilde{u}) - b(\hat{\mathbf{w}}_h - \mathbf{w}, P_k \tilde{u}), \end{aligned}$$

where we have used the first equation of system (14). Moreover, testing the second equation in Problem 2.3 and (13) with $P_k \tilde{u} \in \mathbf{Q}_h$, we have $b(\widehat{\mathbf{w}}_h - \mathbf{w}, P_k \tilde{u}) = 0$, and hence

$$\|\widehat{u}_h - P_k u\|_{0,\Omega}^2 = A_I + A_{II} - b(\widehat{\mathbf{w}}_h - \mathbf{w}, \tilde{u} - P_k \tilde{u}).$$

Our next task is to estimate each terms on the right hand side of the identity above. We begin with A_I .

$$\begin{aligned} A_I &= a_h(\widehat{\mathbf{w}}_h - \Pi_h \mathbf{w}, \tilde{\mathbf{w}}_I - \Pi_h \tilde{\mathbf{w}}) + a(\widehat{\mathbf{w}}_h - \Pi_h \mathbf{w}, \Pi \tilde{\mathbf{w}} - \tilde{\mathbf{w}}_I) \\ &\lesssim \|\widehat{\mathbf{w}}_h - \Pi_h \mathbf{w}\|_{0,\Omega} \|\tilde{\mathbf{w}}_I - \Pi \tilde{\mathbf{w}}\|_{0,\Omega} \\ &\lesssim (\|\widehat{\mathbf{w}}_h - \mathbf{w}\|_{0,\Omega} + \|\mathbf{w} - \Pi_h \mathbf{w}\|_{0,\Omega}) (\|\tilde{\mathbf{w}}_I - \tilde{\mathbf{w}}\|_{0,\Omega} + \|\tilde{\mathbf{w}} - \Pi_h \tilde{\mathbf{w}}\|_{0,\Omega}) \\ (17) \quad &\lesssim h^{\tilde{r}} (\|\widehat{\mathbf{w}}_h - \mathbf{w}\|_{0,\Omega} + \|\mathbf{w} - \Pi_h \mathbf{w}\|_{0,\Omega}) \|\widehat{u}_h - P_k u\|_{0,\Omega}, \end{aligned}$$

where we have applied Lemmas 3.1 and 3.3 and (15). Now, for A_{II} we have

$$(18) \quad A_{II} = a(\widehat{\mathbf{w}}_h - \mathbf{w}, \tilde{\mathbf{w}}_I - \tilde{\mathbf{w}}) \lesssim h^{\tilde{r}} \|\mathbf{w} - \widehat{\mathbf{w}}_h\|_{0,\Omega} \|\widehat{u}_h - P_k u\|_{0,\Omega},$$

and finally, invoking (15), we obtain

$$(19) \quad b(\widehat{\mathbf{w}}_h - \mathbf{w}, \tilde{u} - P_k \tilde{u}) \lesssim h^{\tilde{r}} \|\operatorname{div}(\widehat{\mathbf{w}}_h - \mathbf{w})\|_{0,\Omega} \|\widehat{u}_h - P_k u\|_{0,\Omega}.$$

Collecting (17), (18) and (19), we have

$$\|\widehat{u}_h - P_k u\|_{0,\Omega} \lesssim h^{\tilde{r}} (\|\mathbf{w} - \widehat{\mathbf{w}}_h\|_{\operatorname{div},\Omega} + \|\mathbf{w} - \Pi_h \mathbf{w}\|_{0,\Omega}),$$

concluding the proof. \square

The following auxiliar result shows that the term $\|\mathbf{w} - \widehat{\mathbf{w}}_h\|_{\operatorname{div},\Omega}$ is bounded.

Lemma 3.6. *Let (λ, \mathbf{w}, u) be a solution of Problem 2.3 and $(\widehat{\mathbf{w}}_h, \widehat{u}_h)$ be a solution of (13). Then, there holds*

$$\|\mathbf{w} - \widehat{\mathbf{w}}_h\|_{\operatorname{div},\Omega} \lesssim h^r,$$

with $r > 1/2$ as in Lemma 2.1 and the hidden constant is independent of h .

Proof. Let $(\lambda_h, \mathbf{w}_h, u_h)$ be solution of Problem 3.2. Now, subtracting (13) from Problem 3.2 we obtain

$$\begin{cases} a_h(\mathbf{w}_h - \widehat{\mathbf{w}}_h, \boldsymbol{\tau}_h) + b(\boldsymbol{\tau}_h, u_h - \widehat{u}_h) &= 0 & \forall \boldsymbol{\tau}_h \in \mathbf{H}_h, \\ b(\mathbf{w}_h - \widehat{\mathbf{w}}_h, v_h) &= (\lambda u - \lambda_h u_h, v_h)_{0,\Omega} & \forall v_h \in \mathbf{Q}_h. \end{cases}$$

First, using the inf-sup condition for bilinear form $b(\cdot, \cdot)$ (cf. (3)) we have

$$\|u_h - \widehat{u}_h\|_{0,\Omega} \leq \|\mathbf{w}_h - \widehat{\mathbf{w}}_h\|_{0,\Omega}.$$

Thus,

$$\|\mathbf{w}_h - \widehat{\mathbf{w}}_h\|_{0,\Omega} \lesssim \|\lambda_h u_h - \lambda u\|_{0,\Omega}.$$

Moreover from the second equation, we get

$$\|\operatorname{div}(\mathbf{w}_h - \widehat{\mathbf{w}}_h)\|_{0,\Omega} \leq \|\lambda_h u_h - \lambda u\|_{0,\Omega}.$$

On the other hand, from the triangle inequality and the above estimates, we obtain

$$\begin{aligned} \|\mathbf{w} - \widehat{\mathbf{w}}_h\|_{\operatorname{div},\Omega} &\leq \|\mathbf{w} - \mathbf{w}_h\|_{\operatorname{div},\Omega} + \|\mathbf{w}_h - \widehat{\mathbf{w}}_h\|_{\operatorname{div},\Omega} \\ &\lesssim \|\mathbf{w} - \mathbf{w}_h\|_{\operatorname{div},\Omega} + \|\lambda_h u_h - \lambda u\|_{0,\Omega} \\ &\lesssim \|\mathbf{w} - \mathbf{w}_h\|_{\operatorname{div},\Omega} + |\lambda_h - \lambda| \|u_h\|_{0,\Omega} + |\lambda| \|u_h - u\|_{0,\Omega}, \end{aligned}$$

where using (12) we conclude the proof. \square

We have the following essential identity to conclude the superconvergence result presented in Lemma 3.7.

$$\begin{aligned} (20) \quad -\lambda_h(\widehat{u}_h, u_h) &= -\lambda_h(u_h, \widehat{u}_h) = b(\mathbf{w}_h, \widehat{u}_h) \\ &= -a_h(\widehat{\mathbf{w}}_h, \mathbf{w}_h) = -a_h(\mathbf{w}_h, \widehat{\mathbf{w}}_h) = b(\widehat{\mathbf{w}}_h, u_h) = -\lambda(u, u_h). \end{aligned}$$

Lemma 3.7. *Let (λ, \mathbf{w}, u) and $(\lambda_h, \mathbf{w}_h, u_h)$ be solutions of Problems 2.3 and 3.2, respectively, with $\|u\|_{0,\Omega} = \|u_h\|_{0,\Omega} = 1$. Then, there holds*

$$\|P_k u - u_h\|_{0,\Omega} \lesssim h^{2\tilde{r}},$$

where $\tilde{r} \in (\frac{1}{2}, 1]$ and the hidden constant are independent of h .

Proof. Let $(\hat{\mathbf{w}}_h, \hat{u}_h)$ be the solution of (13). From the triangle inequality we have

$$(21) \quad \|P_k u - u_h\|_{0,\Omega} \leq \|P_k u - \hat{u}_h\|_{0,\Omega} + \|\hat{u}_h - u_h\|_{0,\Omega}.$$

Now, adapting the arguments of [14, Lemma 11] and using (20), we derive the following estimate

$$\|\hat{u}_h - u_h\|_{0,\Omega}^2 \lesssim \|\hat{u}_h - P_k u\|_{0,\Omega}^2 + [\|\mathbf{w} - \mathbf{w}_h\|_{\text{div},\Omega}^2 + \|u - u_h\|_{0,\Omega}^2 + \|\mathbf{w} - \Pi_h \mathbf{w}\|_{0,\Omega}^2]^2.$$

Finally, from (21), the above estimate, together with Lemmas 3.4, 3.5, 3.6, and Theorem 3.1, we conclude the proof. \square

4. A POSTERIORI ERROR ANALYSIS

In this section, we develop an a posteriori error estimator for the acoustic eigenvalue problem (1). The a posteriori error estimator that we will propose is of residual type and our goal is to prove that is reliable and efficient.

Let us introduce some notations and definitions. For any polygon $K \in \mathcal{T}_h$ we denote by \mathcal{E}_K the set of edges of K and

$$\mathcal{E} := \bigcup_{K \in \mathcal{T}_h} \mathcal{E}_K.$$

We decompose \mathcal{E} as $\mathcal{E} := \mathcal{E}_\Omega \cup \mathcal{E}_\Gamma$, where $\mathcal{E}_\Gamma := \{\ell \in \mathcal{E} : \ell \subset \Gamma\}$ and $\mathcal{E}_\Omega := \mathcal{E} \setminus \mathcal{E}_\Gamma$. On the other hand, given $\boldsymbol{\xi} \in L^2(\Omega)^2$, for each $K \in \mathcal{T}_h$ and $\ell \in \mathcal{E}_\Omega$, we denote by $\llbracket \boldsymbol{\xi} \cdot \mathbf{t} \rrbracket$ the tangential jump of $\boldsymbol{\xi}$ across ℓ , that is $\llbracket \boldsymbol{\xi} \cdot \mathbf{t} \rrbracket := (\boldsymbol{\xi}|_K - \boldsymbol{\xi}|_{K'})|_\ell \cdot \mathbf{t}$, where K and K' are elements of \mathcal{T}_h having ℓ as a common edge. Due the regularity assumptions on the mesh, for each polygon $K \in \mathcal{T}_h$ there is a sub-triangulation \mathcal{T}_h^K obtained by joining each vertex of K with the midpoint of the ball with respect to which K is star-shaped. We define

$$\hat{\mathcal{T}}_h := \bigcup_{K \in \mathcal{T}_h} \mathcal{T}_h^K.$$

For each polygon K , we define the following computable and local terms

$$(22) \quad \mathbf{R}_K^2 := h_K^2 \left\| \text{rot } \Pi_h^K \mathbf{w}_h \right\|_{0,K}^2, \quad \boldsymbol{\theta}_K^2 := S^K(\mathbf{w}_h - \Pi_h^K \mathbf{w}_h, \mathbf{w}_h - \Pi_h^K \mathbf{w}_h), \quad \mathbf{J}_\ell := \llbracket \Pi_h^K \mathbf{w}_h \cdot \mathbf{t} \rrbracket,$$

which allows us to define the local error indicator

$$(23) \quad \eta_K := \mathbf{R}_K^2 + \boldsymbol{\theta}_K^2 + \sum_{\ell \in \mathcal{E}_K} h_K \|\mathbf{J}_\ell\|_{0,\ell}^2,$$

and hence, the global error estimator

$$(24) \quad \eta := \left\{ \sum_{K \in \mathcal{T}_h} \eta_K^2 \right\}^{1/2}.$$

In what follows we will prove that (24) is reliable and locally efficient. With this aim, we begin by decomposing the error $\mathbf{w} - \mathbf{w}_h$, using the classical Helmholtz decomposition as follows:

$$\mathbf{w} - \mathbf{w}_h = \nabla \psi + \text{curl } \beta,$$

with $\psi \in \tilde{H}^1(\Omega) := \{v \in H^1(\Omega) : (v, 1)_{0,\Omega} = 0\}$ and $\beta \in H_0^1(\Omega)$. Moreover, the following regularity result holds

$$(25) \quad \|\psi\|_{1,\Omega} + \|\text{curl } \beta\|_{0,\Omega} \lesssim \|\mathbf{w} - \mathbf{w}_h\|_{0,\Omega}.$$

With this decomposition at hand, we split the $L^2(\Omega)$ -norm of the error $\mathbf{w} - \mathbf{w}_h$ into two terms,

$$(26) \quad \|\mathbf{w} - \mathbf{w}_h\|_{0,\Omega}^2 = (\mathbf{w} - \mathbf{w}_h, \nabla \psi)_{0,\Omega} + (\mathbf{w} - \mathbf{w}_h, \mathbf{curl} \beta)_{0,\Omega}.$$

To conclude the reliability, we begin by proving the following results

Lemma 4.1. *There holds*

$$(\mathbf{w} - \mathbf{w}_h, \nabla \psi)_{0,\Omega} \lesssim h^{2\tilde{r}} \|\mathbf{w} - \mathbf{w}_h\|_{0,\Omega},$$

where $\tilde{r} \in (\frac{1}{2}, 1]$ and the hidden constant are independent of h .

Proof. An integration by parts reveals that

$$(\mathbf{w} - \mathbf{w}_h, \nabla \psi)_{0,\Omega} = -(\operatorname{div}(\mathbf{w} - \mathbf{w}_h), \psi)_{0,\Omega} + ((\mathbf{w} - \mathbf{w}_h) \cdot \mathbf{n}, \psi)_{0,\Gamma}.$$

Using that $(\mathbf{w} - \mathbf{w}_h) \cdot \mathbf{n} = 0$ on Γ , the fact that $\operatorname{div} \mathbf{w} = -\lambda u$, $\operatorname{div} \mathbf{w}_h = -\lambda_h u_h$, and adding and subtracting $\lambda_h(u - P_k u, \psi)_{0,\Omega}$, we obtain

$$(\mathbf{w} - \mathbf{w}_h, \nabla \psi)_{0,\Omega} = \underbrace{((\lambda - \lambda_h)u, \psi)_{0,\Omega}}_{\mathbf{I}} + \underbrace{\lambda_h(u - P_k u, \psi)_{0,\Omega}}_{\mathbf{II}} + \underbrace{\lambda_h(P_k u - u_h, \psi)_{0,\Omega}}_{\mathbf{III}}.$$

For the term **I**, we use (12), the fact that $\|u\|_{0,\Omega} = 1$ and (25) in order to obtain

$$(\lambda - \lambda_h)(u, \psi)_{0,\Omega} \lesssim h^{2\min\{r, k+1\}} \|\psi\|_{0,\Omega} \lesssim h^{2\min\{r, k+1\}} \|\mathbf{w} - \mathbf{w}_h\|_{0,\Omega},$$

with $r > \frac{1}{2}$ as in Lemma 2.1. Applying the approximation properties (11) and (25) on **II**, we obtain

$$(u - P_k u, \psi)_{0,\Omega} = (u - P_k u, \psi - P_k \psi)_{0,\Omega} \lesssim h \|u - P_k u\|_{0,\Omega} \|\psi\|_{1,\Omega} \lesssim h^2 \|\mathbf{w} - \mathbf{w}_h\|_{0,\Omega}.$$

Finally, for **III**, we use Lemma 3.7 and the bound for $\|\psi\|_{0,\Omega}$ to write

$$\lambda_h(P_k u - u_h, \psi)_{0,\Omega} \lesssim h^{2\tilde{r}} \|\mathbf{w} - \mathbf{w}_h\|_{0,\Omega}.$$

Now combining the above estimates we conclude the proof. \square

Given $k \in \mathbb{N} \cup \{0\}$, let us consider the following virtual discrete subspace of $H^1(\Omega)$

$$V_h := \{\zeta \in H^1(\Omega) : \Delta \zeta \in \mathbb{P}_{k-1}(\mathbf{K}) \quad \forall \mathbf{K} \in \mathcal{T}_h, \zeta \in \mathcal{C}(\partial \mathbf{K}) : \zeta|_\ell \in \mathbb{P}_{k+1}(\ell), \quad \forall \text{ edge } \ell \subset \partial \mathbf{K}\}.$$

Then, there exists $\zeta_I \in V_h$ that satisfies (see the proof of [35, Lemma 3.4])

$$\|\zeta - \zeta_I\|_{0,\ell} \lesssim h_\ell^{1/2} \|\zeta\|_{1,\mathbf{K}} \quad \text{and} \quad \|\zeta - \zeta_I\|_{0,\mathbf{K}} \lesssim h_{\mathbf{K}} \|\zeta\|_{1,\mathbf{K}} \quad \forall \zeta \in H^1(\mathbf{K}).$$

With this result at hand, now we prove the following result.

Lemma 4.2. *There holds*

$$(\mathbf{w} - \mathbf{w}_h, \mathbf{curl} \beta)_{0,\Omega} \lesssim \eta \|\mathbf{curl} \beta\|_{0,\Omega},$$

where the hidden constant is independent of h and the discrete solution.

Proof. Since $\mathbf{curl} \beta \in H_0(\operatorname{div}^0; \Omega)$, we have that $(\mathbf{w}, \mathbf{curl} \beta)_{0,\Omega} = 0$. Thus,

$$(27) \quad (\mathbf{w} - \mathbf{w}_h, \mathbf{curl} \beta)_{0,\Omega} = (\mathbf{w}_h, \mathbf{curl} \beta)_{0,\Omega} = (\mathbf{w}_h - \Pi_h \mathbf{w}_h, \mathbf{curl} \beta)_{0,\Omega} + (\Pi_h \mathbf{w}_h, \mathbf{curl} \beta)_{0,\Omega}.$$

For the first term on the right-hand side of the above equality we have

$$(28) \quad (\mathbf{w}_h - \Pi_h \mathbf{w}_h, \mathbf{curl} \beta)_{0,\Omega} \lesssim \eta \|\mathbf{curl} \beta\|_{0,\Omega}.$$

Next, we introduce β_I as the virtual interpolant of β , and using that $\mathbf{curl} \beta_h \in H_0(\operatorname{div}^0; \Omega)$, we have

$$(\Pi_h^K \mathbf{w}_h, \mathbf{curl} \beta)_{0,\Omega} = (\Pi_h^K \mathbf{w}_h, \mathbf{curl}(\beta - \beta_I))_{0,\Omega} = \sum_{\mathbf{K} \in \mathcal{T}_h} \int_{\mathbf{K}} \Pi_h^K \mathbf{w}_h \cdot \mathbf{curl}(\beta - \beta_I).$$

Now, by using integration by parts, we obtain

$$(\Pi_h^K \mathbf{w}_h, \mathbf{curl} \beta)_{0,\Omega} = \sum_{\mathbf{K} \in \mathcal{T}_h} \left(\int_{\mathbf{K}} \operatorname{rot} \Pi_h^K \mathbf{w}_h (\beta - \beta_I) + \int_{\partial \mathbf{K}} (\Pi_h^K \mathbf{w}_h \cdot \mathbf{t})(\beta - \beta_I) \right).$$

Hence, applying Cauchy-Schwarz inequality and property of approximation of β_I in the estimate above yields to

$$(29) \quad (\Pi_h^K \mathbf{w}_h, \mathbf{curl} \beta)_{0,\Omega} \lesssim \sum_{K \in \mathcal{T}_h} \eta_K \|\beta\|_{1,\omega_K} \leq C \eta \|\mathbf{curl} \beta\|_{0,\Omega}.$$

Now, combining (27), (28) and (29) we conclude the proof. \square

We now provide an upper bound for our error estimator.

Lemma 4.3. *The following error estimate holds*

$$\|\mathbf{w} - \mathbf{w}_h\|_{0,\Omega} \lesssim \eta + h^{2\tilde{r}},$$

where the hidden constants are independent of h and the discrete solution.

Proof. The proof is a consequence of (26), Lemmas 4.1 and 4.2, together to (25). \square

Thanks to the previous lemmas, we have the following result

Lemma 4.4. *The following error estimate holds*

$$\|\mathbf{w} - \Pi_h \mathbf{w}_h\|_{0,\Omega} \lesssim \eta + h^{2\tilde{r}},$$

where the hidden constant is independent of h .

Proof. From the triangle inequality, together to (10), for the stability of the Π_h -projector and Lemma 4.3, we have

$$\begin{aligned} \|\mathbf{w} - \Pi_h \mathbf{w}_h\|_{0,\Omega} &\leq \|\mathbf{w} - \mathbf{w}_h\|_{0,\Omega} + \|\mathbf{w}_h - \Pi_h \mathbf{w}_h\|_{0,\Omega} \\ &\lesssim \eta + h^{2\tilde{r}}. \end{aligned}$$

Hence, we conclude the proof. \square

Now we are in position to establish the reliability of our estimator.

Corollary 4.1. *[Reliability] The following error estimate hold*

$$\|\mathbf{w} - \mathbf{w}_h\|_{0,\Omega} + \|\mathbf{w} - \Pi_h \mathbf{w}_h\|_{0,\Omega} \lesssim \eta + h^{2\tilde{r}}.$$

where the hidden constants are independent of h .

Remark 4.1. *From Corollary 4.1, we note that $\mathcal{O}(h^{2\tilde{r}})$ can be considered a “higher order term” when lowest order VEM ($k = 0$) is used. When $k \geq 1$, the term can be considered a “higher order term” when the eigenfunction is singular. This usually happens when the eigenproblem is solved in non-convex polygonal domains.*

4.1. Efficiency. Now our aim is to prove that the local indicator η_K defined in (23) provides a lower bound of the error $\mathbf{w} - \mathbf{w}_h$ in a vicinity of any polygon K . To do this task, we proceed as is customary for the efficiency analysis, using suitable bubble functions for the polygons and their edges.

The bubble functions that we will consider are based in [16]. Let $\psi_K \in H_0^1(\Omega)$ be an interior bubble function defined in a polygon K . These bubble functions can be constructed piecewise as the sum of the cubic bubble functions for each triangle of the sub-triangulation \mathcal{T}_h^K that attain the value 1 at the barycenter of each triangle. Also, the edge bubble function $\psi_\ell \in \partial K$ is a piecewise quadratic function attaining the value of 1 at the barycenter of ℓ and vanishing on the triangles $K \in \widehat{\mathcal{T}}_h$ that do not contain ℓ on its boundary.

The following technical results for the bubble functions are a key point to prove the efficiency bound.

Lemma 4.5. *For any $K \in \mathcal{T}_h$, let ψ_K be the corresponding interior bubble function. Then, there hold*

$$\begin{aligned} \|p\|_{0,K}^2 &\lesssim \int_K \psi_K p^2 \lesssim \|p\|_{0,K}^2 \quad \forall p \in \mathbb{P}_k(K); \\ \|p\|_{0,K} &\lesssim \|\psi_K p\|_{0,K} + h_K \|\nabla(\psi_K p)\|_{0,K} \lesssim \|p\|_{0,K} \quad \forall p \in \mathbb{P}_k(K); \end{aligned}$$

where the hidden constants are independent of h_K

Lemma 4.6. *For any $K \in \mathcal{T}_h$ and $\ell \in \mathcal{E}_K$, let ψ_ℓ be the corresponding edge bubble function. Then, there holds*

$$\|p\|_{0,\ell}^2 \lesssim \int_\ell \psi_\ell p^2 \lesssim \|p\|_{0,\ell}^2 \quad \forall p \in \mathbb{P}_k(\ell).$$

Moreover, for all $p \in \mathbb{P}_k(\ell)$, there exists an extension of $p \in \mathbb{P}_k(K)$, which we denote simply by p , such that

$$h_K^{-1/2} \|\psi_\ell p\|_{0,K} + h_K^{1/2} \|\nabla(\psi_\ell p)\|_{0,K} \lesssim \|p\|_{0,\ell},$$

where the hidden constants are independent of h_K .

Now we are in position to establish the main result of this section.

Theorem 4.1. *For any $K \in \mathcal{T}_h$, there holds*

$$\eta_K \lesssim \|\mathbf{w}_h - \mathbf{w}\|_{0,\omega_\ell} + \|\mathbf{w} - \Pi_h^K \mathbf{w}_h\|_{0,\omega_\ell},$$

where ω_ℓ denotes the union of two polygons sharing an edge with K , and the hidden constant is independent of h and the discrete solution.

Proof. The aim is to estimate each term of the local indicator (23). The proof is divided in three steps:

- **Step 1:** We begin by estimating R_K^2 in (22). Invoking the properties of the bubble function ψ_K , Cauchy-Schwarz inequality, and Lemma 4.5, we have

$$\begin{aligned} R_K^2 &\lesssim \int_K \psi_K \operatorname{rot}(\Pi_h^K \mathbf{w}_h) \operatorname{rot}(\Pi_h^K \mathbf{w}_h) = \int_K \psi_K \operatorname{rot}(\Pi_h^K \mathbf{w}_h) \operatorname{rot}(\Pi_h^K \mathbf{w}_h - \mathbf{w}_h) \\ &= - \int_K (\Pi_h^K \mathbf{w}_h - \mathbf{w}_h) \operatorname{curl}(\psi_K \operatorname{rot}(\Pi_h^K \mathbf{w}_h)) \lesssim \|\Pi_h^K \mathbf{w}_h - \mathbf{w}_h\|_{0,K} h_K^{-1} \|\operatorname{rot}(\Pi_h^K \mathbf{w}_h)\|_{0,K}, \end{aligned}$$

which implies that

$$(30) \quad R_K = h_K \|\operatorname{rot}(\Pi_h^K \mathbf{w}_h)\|_{0,K} \lesssim \|\mathbf{w} - \mathbf{w}_h\|_{0,K} + \|\mathbf{w} - \Pi_h^K \mathbf{w}_h\|_{0,K}.$$

- **Step 2:** Now we estimate J_h . Following the proof of [17, Lemma 5.16], we obtain

$$\|J_\ell\|_{0,\ell}^2 \lesssim \|\psi_\ell J_\ell\|_{0,\ell}^2 = \int_\ell (\psi_\ell J_\ell) \cdot J_\ell = \int_{\omega_\ell} (\mathbf{w} - \Pi_h^K \mathbf{w}_h) \cdot \operatorname{curl}(\psi_\ell J_\ell) + \int_{\omega_\ell} \psi_\ell J_\ell \operatorname{rot} \Pi_h^K \mathbf{w}_h.$$

Hence, from Cauchy-Schwarz inequality, the bubble function properties and (30), we have

$$\begin{aligned} \|J_\ell\|_{0,\ell}^2 &\lesssim |\psi_\ell J_\ell|_{1,\omega_\ell} \|\mathbf{w} - \Pi_h^K \mathbf{w}_h\|_{0,\omega_\ell} + \|\psi_\ell J_\ell\|_{0,\omega_\ell} \|\operatorname{rot} \Pi_h^K \mathbf{w}_h\|_{0,\omega_\ell}, \\ &\lesssim h_K^{-1/2} \left(\|\mathbf{w}_h - \mathbf{w}\|_{0,\omega_\ell} + \|\mathbf{w} - \Pi_h^K \mathbf{w}_h\|_{0,\omega_\ell} \right) \|J_\ell\|_{0,\ell}. \end{aligned}$$

Hence, we conclude that

$$(31) \quad h_K^{1/2} \|J_\ell\|_{0,\ell} \lesssim \|\mathbf{w}_h - \mathbf{w}\|_{0,\omega_\ell} + \|\mathbf{w} - \Pi_h^K \mathbf{w}_h\|_{0,\omega_\ell}.$$

- **Step 3:** The final step is to control the term θ_K . To do this task, we use the stability property (10), add and subtract \mathbf{w} with the purpose of applying triangular inequality as follows

$$(32) \quad \theta_K \leq c_1 \|\mathbf{w}_h - \Pi_h^K \mathbf{w}_h\|_{0,K} \lesssim \|\mathbf{w}_h - \mathbf{w}\|_{0,K} + \|\Pi_h^K \mathbf{w}_h - \mathbf{w}\|_{0,K}.$$

Hence, the proof is complete by gathering (30), (31) and (32). \square

As a direct consequence of lemma above, we have the following result that allows us to conclude the efficiency of the local and global error estimators for the acoustic problem, and hence, for its equivalent mixed problem.

Corollary 4.2. *[Efficiency] There holds*

$$\eta \lesssim \|\mathbf{w} - \mathbf{w}_h\|_{0,\Omega} + \|\mathbf{w} - \Pi_h \mathbf{w}_h\|_{0,\Omega},$$

where the hidden constants are independent of h .

5. NUMERICAL RESULTS

In this section, we report numerical tests in order to assess the behavior of the a posteriori estimator defined in (24). With this aim, we have implemented in a MATLAB code a lowest order VEM scheme on arbitrary polygonal meshes.

We have used the mesh refinement algorithm described in [7], which consists in splitting each element of the mesh into n quadrilaterals (n being the number of edges of the polygon) by connecting the barycenter of the element with the midpoint of each edge, which will be named as **Adaptive VEM**. Notice that although this process is initiated with a mesh of triangles, the successively created meshes will contain other kind of convex polygons, as it can be seen in Figure 1. Both schemes are based on the strategy of refining those elements $K \in \mathcal{T}_h$ that satisfy

$$\eta_K \geq 0.5 \max_{K' \in \mathcal{T}_h} \{\eta_{K'}\}.$$

5.1. Test 1: L-shaped domain. We will consider the non-convex domain $\Omega := (0,1) \times (0,1) \setminus [1/2, 1] \times [1/2, 1]$.

It is clear that the first eigenfunction of the acoustic problem in this domain is not smooth enough, due the presence of a geometrical singularity at $(\frac{1}{2}, \frac{1}{2})$. This leads to a lack of regularity due to the reentrant angle $\omega = \pi/3$. Therefore, according to [9], using quasi-uniform meshes, the convergence rate for the eigenvalues should be $|\lambda - \lambda_h| = \mathcal{O}(h^{4/3}) \approx \mathcal{O}(N^{-2/3})$, where N denotes the number of degrees of freedom. Then, the proposed a posteriori estimator (24) must be capable to recover the optimal order $|\lambda - \lambda_h| = \mathcal{O}(N^{-1})$, when the adaptive refinement is performed near to the singularity point.

For the numerical tests, we have computed the smallest eigenvalue and its corresponding eigenfunction using the MATLAB command `eigs`.

Figures 1 to 2 show the adaptively refined meshes obtained with VEM procedures and different initial meshes. Figure 1 is initiated with a mesh of triangles, while Figure 2 is initiated with a non-structured hexagonal meshes made of convex hexagons.

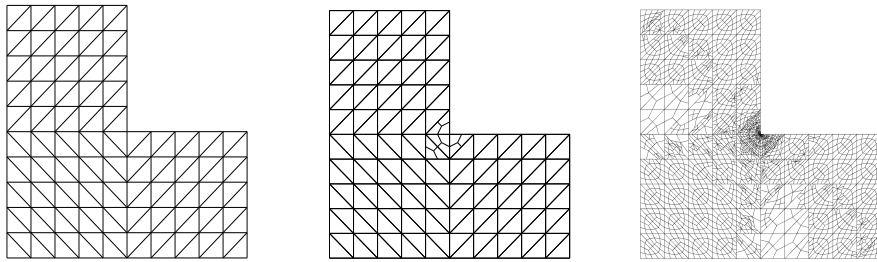


FIGURE 1. Test 1. Adaptively refined meshes obtained with VEM scheme at refinement steps 0, 1 and 8 (Adaptive VEM).

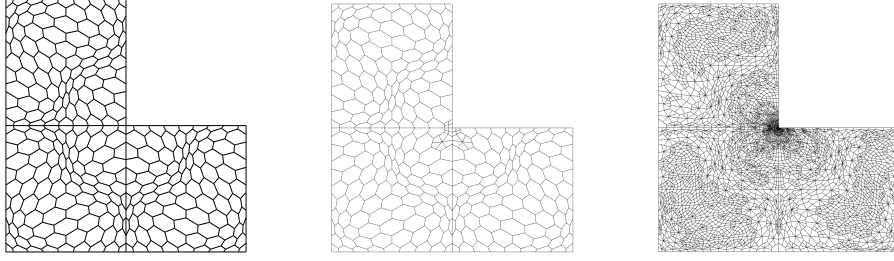


FIGURE 2. Test 1. Adaptively refined meshes obtained with VEM scheme at refinement steps 0, 1 and 8 (Adaptive VEM).

Figures 1 and 2 show that our estimator identifies the singularity point of the domain, leading to a refinement on the region of the re-entrant angle. This refinement allows to achieve the optimal order of convergence for the eigenvalue.

In order to compute the errors $|\lambda_1 - \lambda_{h1}|$, and since an exact eigenvalue is not known, we have used an approximation based on a least-squares fitting of the computed values obtained with extremely refined meshes. Thus, we have obtained the value $\lambda_1 = 5.9017$, which has at least four accurate significant digits.

We report in Table 1 the lowest eigenvalue λ_{h1} on uniformly refined meshes, adaptively refined meshes with VEM schemes and in the last column we report adaptively refined meshes with VEM schemes and initial non-structured hexagonal meshes. Each table includes the estimated convergence rate.

TABLE 1. Test 1. Computed lowest eigenvalue λ_{h1} computed with different schemes.

Uniform VEM		Adaptive VEM		Adaptive VEMH	
N	λ_{h1}	N	λ_{h1}	N	λ_{h1}
245	5.6831	245	5.6831	829	5.8283
940	5.8231	266	5.7356	872	5.8495
3680	5.8732	288	5.7554	945	5.8605
14560	5.8914	381	5.7805	1131	5.8688
57920	5.8982	889	5.8440	2010	5.8833
231040	5.9008	1206	5.8620	3296	5.8895
		1731	5.8713	4932	5.8928
		3639	5.8876	7287	5.8955
		5206	5.8924	12003	5.8982
		7653	5.8949	19349	5.8998
		14545	5.8985	30751	5.9007
		22982	5.9000	50421	5.9014
		33844	5.9006		
		61641	5.9015		
Order	$\mathcal{O}(N^{-0.79})$	Order	$\mathcal{O}(N^{-1.08})$	Order	$\mathcal{O}(N^{-1.14})$
λ_1	5.9017	λ_1	5.9017	λ_1	5.9017

In Figure 3 we present error curves where we observe that the two refinement schemes lead to a correct convergence rate. It can be seen from Table 1 and Figure 3, that the uniform refinement leads to a convergence rate close to that predicted by the theory, while the adaptive VEM schemes allow us to recover the optimal order of convergence $\mathcal{O}(N^{-1})$.

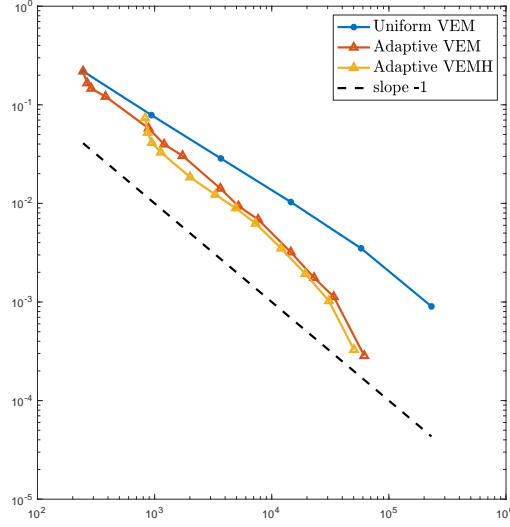


FIGURE 3. Test 1. Error curves of $|\lambda_1 - \lambda_{h1}|$ for uniformly refined meshes (“Uniform VEM”), adaptively refined meshes with VEM (“Adaptive VEM”) and adaptively refined meshes with VEM and initial mesh of hexagons (“Adaptive VEMH”).

We report in Table 2, the error $|\lambda_1 - \lambda_{h1}|$ and the estimators $\boldsymbol{\eta}$ at each step of the adaptive VEM scheme. We include in the table the terms $\boldsymbol{\theta}^2 := \sum_{K \in \mathcal{T}_h} \boldsymbol{\theta}_K^2$, which appears from the inconsistency of the VEM, and $\mathbf{J}_h := \sum_{K \in \mathcal{T}_h} \left(\sum_{\ell \in \mathcal{E}_K} h_K \|\mathbf{J}_\ell\|_{0,\ell}^2 \right)$, which arise from the edge residuals. We also report in the table the effectivity indexes $|\lambda_1 - \lambda_{h1}|/\boldsymbol{\eta}^2$.

TABLE 2. Components of the error estimator and effectivity indexes on the adaptively refined meshes with VEM.

N	λ_{h1}	$ \lambda_1 - \lambda_{h1} $	$\boldsymbol{\theta}^2$	\mathbf{J}_h^2	$\boldsymbol{\eta}^2$	$\frac{ \lambda_1 - \lambda_{h1} }{\boldsymbol{\eta}^2}$
245	5.6831	2.1869e-01	9.4718e-03	1.3226e-01	1.4174e-01	1.5429
266	5.7356	1.6614e-01	1.2881e-02	8.5612e-02	9.8493e-02	1.6868
288	5.7554	1.4637e-01	1.2791e-02	7.5101e-02	8.7892e-02	1.6653
381	5.7805	1.2119e-01	1.2944e-02	5.6072e-02	6.9016e-02	1.7560
889	5.8440	5.7776e-02	9.4599e-03	1.5576e-02	2.5036e-02	2.3077
1206	5.8620	3.9753e-02	6.8149e-03	1.0962e-02	1.7777e-02	2.2362
1731	5.8713	3.0451e-02	5.1742e-03	8.1822e-03	1.3356e-02	2.2799
3639	5.8876	1.4166e-02	2.7744e-03	3.2286e-03	6.0030e-03	2.3598
5206	5.8924	9.3787e-03	1.8562e-03	2.3210e-03	4.1771e-03	2.2453
7653	5.8949	6.8767e-03	1.3746e-03	1.6477e-03	3.0223e-03	2.2753
14545	5.8985	3.1983e-03	7.4205e-04	9.1237e-04	1.6544e-03	1.9332
22982	5.9000	1.7633e-03	4.6344e-04	5.9698e-04	1.0604e-03	1.6628
33844	5.9006	1.1283e-03	3.3863e-04	4.2666e-04	7.6529e-04	1.4743

From Table 2 we observe that the effectivity indexes are bounded and far from zero. Also, the inconsistency and edge residual terms are, roughly speaking, of the same order. This results are

similar to those obtained in [35]. We end this test presenting in Figure 4 the displacement field and the pressure fluctuation of the fluid on the L-shaped domain, associated to the first eigenfunction.

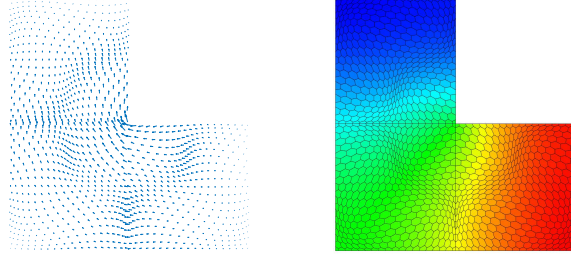


FIGURE 4. Test 1. Eigenfunctions of the acoustic problem corresponding to the first lowest eigenvalue: displacement field \mathbf{w}_{h1} (left), pressure fluctuation p_{h1} (right).

5.2. Test 2: H-shaped domain. The aim of this test is to assess the performance of the adaptive scheme when solving a problem with a singular solution. In this test Ω consists of an H-shaped domain that represents the union of two pools. More precisely, the geometry of this domain is given by

$$\Omega := \{(0, 3/2) \times (0, 3)\} \setminus \{[1/2, 1] \times [0, 5/4]\} \cup \{[1/2, 1] \times [15/8, 3]\}.$$

According to the definition of this domain, four singularities are present, leading once again to a lack of regularity for the eigenfunctions of our acoustic problem. Hence, the proposed estimator $\boldsymbol{\eta}$ defined in (24) must be capable of identify these singularities of the geometry and perform an adaptive refinement, with different polygonal meshes, in order to recover optimal order of convergence.

Figures 5 to 7 show the adaptively refined meshes obtained with VEM procedures and different initial meshes. In Figure 5 we start with a mesh of triangles and squares, while in Figure 6 we begin with a trapezoidal mesh consisting of partitions of the domain into $M \times M$ congruent trapezoids. Finally in Figure 7 we start with a Voronoi mesh.

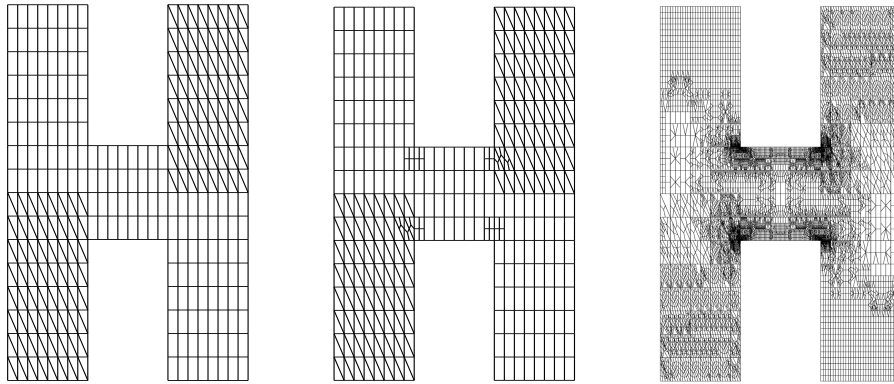


FIGURE 5. Adaptively refined meshes obtained with VEM scheme at refinement steps 0, 1 and 8 (Adaptive VEM S-T).

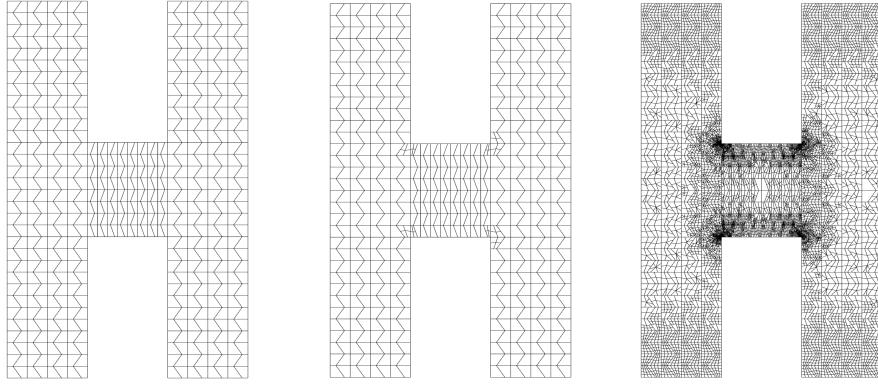


FIGURE 6. Adaptively refined meshes obtained with VEM scheme at refinement steps 0, 1 and 8 (Adaptive VEM B).

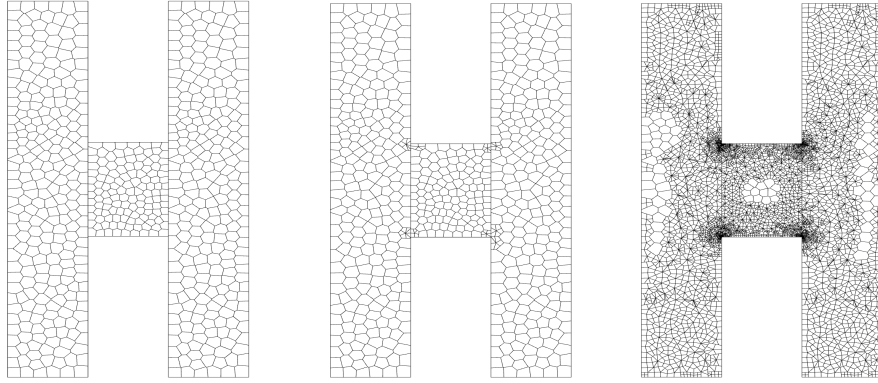


FIGURE 7. Adaptively refined meshes obtained with VEM scheme at refinement steps 0, 1 and 8 (Adaptive VEM V).

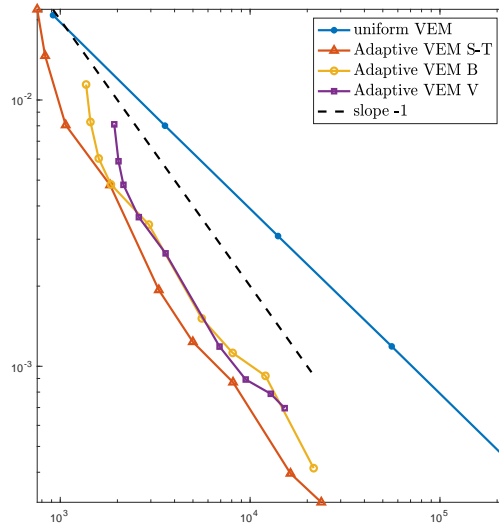
Similarly to Test 1, the computations of the errors $|\lambda_2 - \lambda_{h2}|$, have been obtained with a least squares fitting of the calculated values obtained with extremely refined meshes. Thus, we have obtained the value $\lambda_2 = 1.2040$, which has at least four exact significant digits.

In Table 3 we report the second lowest eigenvalue λ_{h2} on uniformly refined meshes, adaptively refined meshes with different type of initial meshes. Each table includes the estimated convergence rate.

TABLE 3. Computed lowest eigenvalue λ_{h2} computed with different initial meshes.

Uniform VEM		Adaptive VEM S-T		Adaptive VEM B		Adaptive VEM V	
N	λ_{h2}	N	λ_{h2}	N	λ_{h2}	N	λ_{h2}
916	1.1831	756	1.1821	1368	1.1925	1925	1.1959
3560	1.1960	832	1.1893	1442	1.1957	2027	1.1981
14032	1.2009	1068	1.1959	1594	1.1979	2152	1.1992
55712	1.2028	1830	1.1992	1848	1.1991	2593	1.2003
222016	1.2035	3304	1.2020	2928	1.2006	3588	1.2013
		4992	1.2027	5564	1.2024	6903	1.2028
		8130	1.2031	8093	1.2028	9480	1.2031
		16320	1.2036	12045	1.2030	12846	1.2032
		23706	1.2037	21613	1.2036	15214	1.2033
Order	$\mathcal{O}(N^{-0.70})$	Order	$\mathcal{O}(N^{-1.19})$	Order	$\mathcal{O}(N^{-1.09})$	Order	$\mathcal{O}(N^{-1.11})$
λ_2	1.2040	λ_2	1.2040	λ_2	1.2040	λ_2	1.2040

In Figure 8 we present error curves where we observe that the three refinement schemes lead to a correct convergence rate. It can be seen from Table 3 and Figure 8, that the uniform refinement leads to a convergence rate close to that predicted by the theory, while the adaptive VEM schemes allow us to recover the optimal order of convergence $\mathcal{O}(N^{-1})$.

FIGURE 8. Error curves of $|\lambda_2 - \lambda_{h2}|$ for uniformly refined meshes and adaptively refined meshes VEM with different initial meshes.

In Figure 9 we present plots of the computed eigenfunctions \mathbf{w}_{h2} (displacement field) and p_{h2} (pressure fluctuation) corresponding to the second eigenvalue.

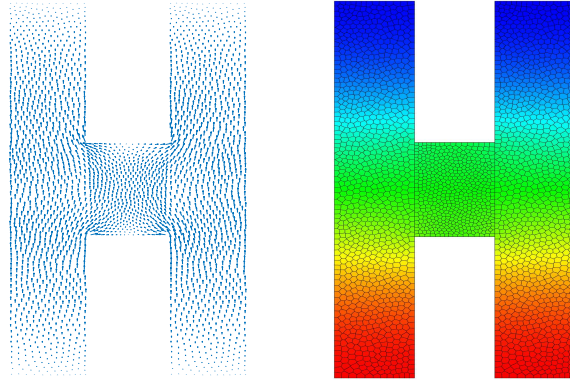


FIGURE 9. Test 2. Eigenfunctions of the acoustic problem corresponding to the second lowest eigenvalue: displacement field \mathbf{w}_{h2} (left), pressure fluctuation p_{h2} (right).

5.3. Test 3: Circular domain with obstacles. As a third test, we have considered a configuration closer to a real application: four square tubes immersed in a fluid occupying a circular cavity. Clearly in this test there are two relevant geometrical issues: in one hand, we have a non polygonal domain for which we are making an approximation by means of polygonal meshes, and the four rigid squares that lie in the interior of the circle. These tubes lead to non smooth eigenfunctions when the solutions for the acoustic problem are approximated, due the singularities of the corner on each square.

To make matters precise, let us define the circular domain by $\Omega_C := \{(x, y) \in \mathbb{R}^2 : x^2 + y^2 < 1\}$ and the squares $\Omega_I := [1/5, 3/5] \times [1/5, 3/5]$, $\Omega_{II} := [-3/5, -1/5] \times [1/5, 3/5]$, $\Omega_{III} := [-3/5, -1/5] \times [-3/5, -1/5]$ and $\Omega_{IV} := [1/5, 3/5] \times [-3/5, -1/5]$. Hence, the computational domain is $\Omega := \Omega_C \setminus \{\Omega_I \cup \Omega_{II} \cup \Omega_{III} \cup \Omega_{IV}\}$.

In the sequel, we consider the fourth eigenfunction. In Figure 10 we present an adaptive refinement of our estimator when Voronoi meshes are considered. On the left hand side we present the initial mesh and, after 1 and 8 iterations of our numerical method, we observe that the estimator η identifies the singularities on the geometry that cause the poor regularity of the eigenfunction, and starts the refinement around these corners in order to recover the optimal order of convergence.

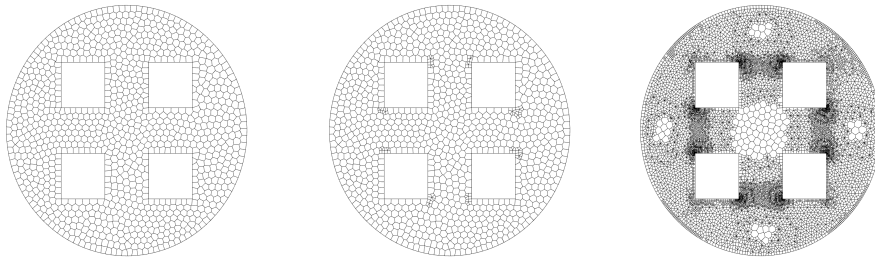


FIGURE 10. Adaptively refined meshes obtained with VEM scheme at refinement steps 0, 1 and 8 (Adaptive VEM V).

Figure 11 shows a logarithmic plot of the errors between the calculated approximations of the fourth smallest positive eigenvalue and the “exact” one, versus the number of degrees of freedom N of the meshes. As in the previous two tests, the exact value of the fourth eigenvalue is obtained by using

a least squares fit. The figure shows the results obtained with "uniform" meshes and with adaptively refined meshes and shows how the optimal order of convergence is recovered. Finally, Figure 12 shows the eigenfunctions of the acoustic problem corresponding to the fourth lowest eigenvalue.

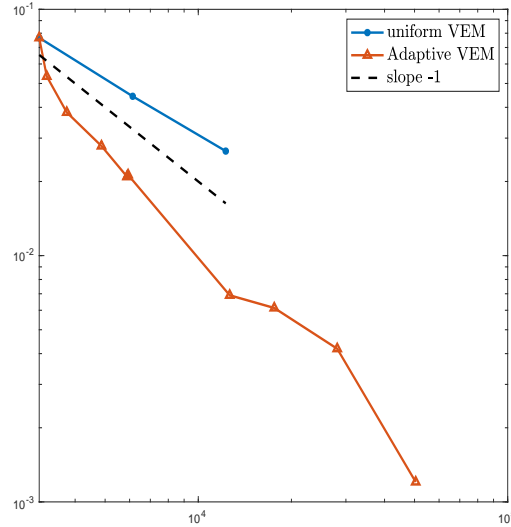


FIGURE 11. Error curves of $|\lambda_4 - \lambda_{h4}|$ for uniformly refined meshes and adaptively refined meshes VEM.

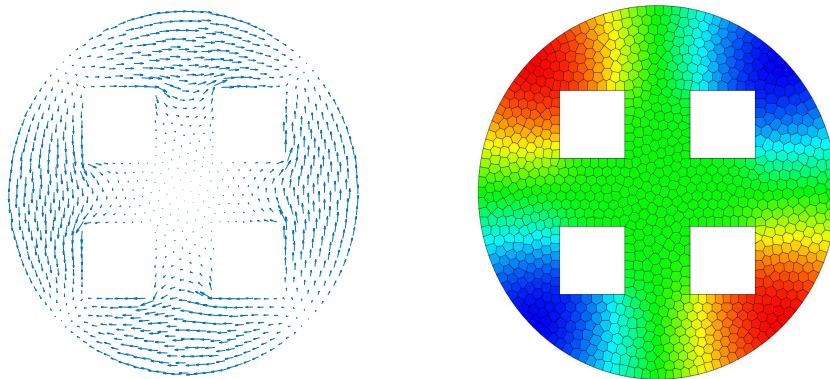


FIGURE 12. Test 3. Eigenfunctions of the acoustic problem corresponding to the second lowest eigenvalue: displacement field \mathbf{w}_{h4} (left), pressure fluctuation p_{h4} (right).

6. CONCLUSIONS

In this work, we have derived and analyzed an a posteriori error estimate for the acoustic vibration problem by means of mixed virtual element discretization. The theoretical analysis developed in this work was strongly supported by superconvergence results for mixed spectral formulations. Several numerical tests that substantiate the theoretical results were presented, confirming that the proposed

estimator is capable of recover the optimal order of convergence, as theory predicts. Moreover, we stress that the present analysis can be extended to the tridimensional case by using the VEM spaces introduced in [6] and the recent results for interpolation estimates derived in [8].

REFERENCES

1. Agmon S., Lectures on Elliptic Boundary Value Problems, Van Nostrand Mathematical Studies, No. 2. D (B. F. Jones Jr & G. W. Batten Jr, eds.). Princeton, NJ; Toronto-London: Van Nostrand, (1965).
2. Alonso A., Russo Dello A. and Vampa V., *A posteriori error estimates in finite element acoustic analysis*, J. Comput. Appl. Math., **117**, (2000), pp.105–119.
3. Babuška I. and Osborn J., Eigenvalue Problems in Handbook of Numerical Analysis, Vol. II, Ciarlet P.G. and Lions J.L., eds., North-Holland, Amsterdam, pp. 641–787, 1991.
4. Beirão da Veiga L., Brezzi F., Cangiani A., Manzini G., Marini L.D. and Russo A., *Basic principles of virtual element methods*, Math. Models Methods Appl. Sci., **23**, (2013), pp. 199–214.
5. Beirão da Veiga L., Brezzi F., Marini L.D. and Russo A., *Mixed virtual element methods for general second order elliptic problems on polygonal meshes*, ESAIM Math. Model. Numer. Anal., **50**, (2016), pp. 727–747.
6. Beirão da Veiga L., Brezzi F., Marini L.D. and Russo A., *H(div) and H(curl)-conforming virtual element methods*, Numer. Math., **133**, (2016), pp. 303–332.
7. Beirão da Veiga L. and Manzini G., *Residual a posteriori error estimation for the virtual element method for elliptic problems*, ESAIM Math. Model. Numer. Anal., **49**, (2015), pp. 577–599.
8. Beirão da Veiga L., Mascotto L. and Meng J., *Interpolation and stability estimates for edge and face virtual elements of general order*, arXiv:2203.00303 [math.NA] (2022).
9. Beirão da Veiga L., Mora D., Rivera G. and Rodríguez R., *A virtual element method for the acoustic vibration problem*, Numer. Math., **136**, (2017), pp. 725–763.
10. Boffi D., Brezzi F. and Fortin M., Mixed Finite Element Methods and Applications, Springer Series in Computational Mathematics, 44. Springer, Heidelberg (2013).
11. Boffi D., Durán R. G., Gardini F. and Gastaldi L., *A posteriori error analysis for nonconforming approximation of multiple eigenvalues*, Math. Methods Appl. Sci., **40**, (2017), pp. 350–369.
12. Boffi D., Gallistl D., Gardini F. and Gastaldi L., *Optimal convergence of adaptive FEM for eigenvalue clusters in mixed form*, Math. Comp., **86**, (2017), pp. 2213–2237.
13. Boffi D., Gastaldi L., Rodríguez R. and Šebestová I., *Residual-based a posteriori error estimation for the Maxwell’s eigenvalue problem*, IMA J. Numer. Anal., **37**, (2017), pp. 1710–1732.
14. Boffi D., Gastaldi L., Rodríguez R. and Šebestová I., *A posteriori error estimates for Maxwell’s eigenvalue problem*, J. Sci. Comput., **78** (2019), pp. 1250–1271.
15. Brezzi F., Falk R. S. and Marini L. D., *Basic principles of mixed virtual element methods*, ESAIM Math. Model. Numer. Anal., **48**, (2014), pp. 1227–1240.
16. Cangiani A., Georgoulis E. H. , Pryer T. and Sutton O. J., *A posteriori error estimates for the virtual element method*, Numer. Math., **137**, (2017), pp. 857–893.
17. Cangiani A. and Munar M., *A posteriori error estimates for mixed virtual element methods*, Pre-print arXiv:1904.10054 [math.NA] (2019).
18. Čertík O., Gardini F., Manzini G., Mascotto L. and Vacca G., *The p- and hp-versions of the virtual element method for elliptic eigenvalue problems*, Comput. Math. Appl., **79**, (2020), pp. 2035–2056.
19. Dassi F. and Velásquez I., *Virtual element method on polyhedral meshes for bi-harmonic eigenvalues problems*, Comput. Math. Appl., **121**, (2022), pp. 85–101.
20. Douglas Jr., J. and Roberts, J.E., *Mixed finite element methods for second order elliptic problems*, Math. Appl. Comput., **1**, (1982), pp. 91–103.
21. Durán R., Gastaldi L. and Padra C., *A posteriori error estimator for mixed approximations of eigenvalue problems*, Math. Models Methods Appl. Sci., **9**, (1999), pp. 1165–1178.
22. Durán R., Padra C. and Rodríguez, R., *A posteriori error estimates for the finite element approximation of eigenvalue problems*, Math. Models Methods Appl. Sci., **13**, (2003), pp. 1219–1229.
23. Gardini, F., *Mixed approximation of eigenvalue problems: a superconvergence result*, ESAIM Math. Model. Numer. Anal., **43**, (2009), pp. 853–865.
24. Gardini F., Manzini G. and Vacca G., *The nonconforming virtual element method for eigenvalue problems*, ESAIM Math. Model. Numer. Anal., **53**, (2019), pp. 749–774.
25. Gardini F. and Vacca G., *Virtual element method for second-order elliptic eigenvalue problems*, IMA J. Numer. Anal., **38**, (2018), pp. 2026–2054.
26. Lepe F. and Rivera G., *A virtual element approximation for the pseudostress formulation of the Stokes eigenvalue problem*, Comput. Methods Appl. Mech. Engrg., **379**, (2021), Paper No. 113753.
27. Lepe F. and Rivera G., *A priori error analysis for a mixed VEM discretization of the spectral problem for the Laplacian operator*, Calcolo, **58**, (2021), pp. 30.
28. Lepe F., Mora D., Rivera G. and Velásquez I., *A virtual element method for the Steklov eigenvalue problem allowing small edges*, J. Sci. Comput., **88**, 44, (2021).
29. Lin Q. and Xie H., *A superconvergence result for mixed finite element approximations of the eigenvalue problem*, ESAIM Math. Model. Numer. Anal., **46**, (2012), pp. 797–812.

30. Meng J. and Mei L., *A mixed virtual element method for the vibration problem of clamped Kirchhoff plate*, Adv. Comput. Math., **46**, (2020), no. 5, Paper No. 68, 18 pp.
31. Meng J., Wang G. and Mei L., *Mixed virtual element method for the Helmholtz transmission eigenvalue problem on polytopal meshes*, IMA J. Numer. Anal., (in press) DOI:10.1093/imanum/drac019
32. Meng J., Zhang Y. and Mei L., *A virtual element method for the Laplacian eigenvalue problem in mixed form*, Appl. Numer. Math., **156**, (2020), pp. 1–13.
33. Mora D. and Rivera G., *A priori and a posteriori error estimates for a virtual element spectral analysis for the elasticity equations*, IMA J. Numer. Anal., **40**, (2020), pp. 322–357.
34. Mora D., Rivera G. and Rodríguez R., *A virtual element method for the Steklov eigenvalue problem*, Math. Models Methods Appl. Sci., **25**, (2015), pp. 1421–1445.
35. Mora D., Rivera G. and Rodríguez R., *A posteriori error estimates for a virtual element method for the Steklov eigenvalue problem*, Comput. Math. Appl., **74**, (2017), pp. 2172–2190.
36. Mora D. and Velásquez I., *Virtual elements for the transmission eigenvalue problem on polytopal meshes*, SIAM J. Sci. Comput., **43**, (2021), pp. A2425–A2447.
37. Munar, M. and Sequeira, F.A., *A posteriori error analysis of a mixed virtual element method for a nonlinear Brinkman model of porous media flow*, Comput. Math. Appl., **80**, (2020), pp. 1240–1259.
38. Verfurth R., *A Review of A Posteriori Error Estimation and Adaptive Mesh-Refinement Techniques*, Chichester: Wiley-Teubner. (1996).
39. Verfurth R., *A Posteriori Error Estimation Techniques for Finite Element Method*, Numerical Mathematics and Scientific Computation, Oxford University Press, Oxford, (2013).
40. Wang G., Meng J., Wang, Y. and Mei L., *A priori and a posteriori error estimates for a virtual element method for the non-self-adjoint Steklov eigenvalue problem*, IMA J. Numer. Anal., (in press) DOI:10.1093/imanum/drab079

GIMNAP-DEPARTAMENTO DE MATEMÁTICA, UNIVERSIDAD DEL BÍO-BÍO, CASILLA 5-C, CONCEPCIÓN, CHILE.

Email address: flepe@ubiobio.cl

GIMNAP-DEPARTAMENTO DE MATEMÁTICA, UNIVERSIDAD DEL BÍO-BÍO, CASILLA 5-C, CONCEPCIÓN, CHILE AND CI²MA, UNIVERSIDAD DE CONCEPCIÓN, CONCEPCIÓN, CHILE.

Email address: dmora@ubiobio.cl

DEPARTAMENTO DE CIENCIAS EXACTAS, UNIVERSIDAD DE LOS LAGOS, CASILLA 933, OSORNO, CHILE.

Email address: gonzalo.rivera@ulagos.cl

DEPARTAMENTO DE CIENCIAS BÁSICAS, UNIVERSIDAD DEL SINÚ ELÍAS BECHARA ZAINÚM, MONTERÍA, COLOMBIA.

Email address: ivanvelasquez@unisinu.edu.co